[PS]Permeability Estimation Based on Pore Characterization and Flow Modeling from Thin-Sections Image Analysis of Grain-Dominated Carbonates*

Sheng Peng[1], Ahmed Hassan[1], and Robert G. Loucks[1]

Search and Discovery Article #42117 (2017)**
Posted August 7, 2017

*Adapted from poster presentation given at 2017 AAPG Annual Convention & Exhibition, Houston, Texas, April 2-5, 2017

[1]BEG, UT Austin, Austin, Texas (sheng.peng@beg.utexas.edu)

Abstract

Image analysis can provide insights regarding pore networks, including pore sizes and types, and can also be useful for permeability estimation. Permeability estimation based on image analysis is a good alternative when intact core-plugs are not available for laboratory measurement. While there is much research on permeability estimation from 2D and 3D images or models, accurately estimating permeability for carbonates, which contains highly variable pore networks, is still challenging. In this study, a method for permeability estimation based on thin-section image analysis and 2D permeability simulation was developed for grain-dominated carbonates based on semi-theoretical analysis of 2D and 3D permeability (K2D and K3D) relationships. The mathematical expression of the K2D/K3D is examined with a carbonate grainstone sample, for which both K2D and K3D were obtained through permeability simulation based on micro-CT images.

The method was applied to 24 grain-dominated carbonate samples collected from different wells in West Texas and Abu Dubai having large variations in rock textures and fabrics and a broad range of permeability from 0.1 mD to 3200 mD. The representativeness of the thin sections and correct determination of the effective pores are key for accurate permeability estimation. When estimated permeability values were compared to measured values, we found that 92% of the estimated results are within a factor of ±5 of the measured values (a factor of 5 means the ratio of estimated over measured permeability equals 5; a factor of -5 means the ratio of estimated over measured permeability equals 1/5), and 46% within a factor of ±2. Two-dimensional image analysis and modeling are simpler than those in 3D, but still include the influence of pore shapes and size distribution. Therefore, this thin-section based method can be used as a quick yet reliable way for permeability estimation.

Permeability Estimation Based on Pore Characterization and Flow Modeling from Thin-Section Image Analysis of Grain-Dominated Carbonates

TEXAS Geosciences
The University of Texas at Austin
Jackson School of Geosciences

Sheng Peng, Ahmed Hassan, Robert G. Loucks

Bureau of Economic Geology, Jackson School of Geosciences, The University of Texas at Austin, Austin, TX

Bureau of Economic Geology
Reservoir Characterization Research Laboratory

Problem Statement and Objectives

- The ability to have an accurate estimate of permeability is important in reservoir characterization. Direct laboratory measurements, while more straightforward, are sometimes limited by the availability of usable core plugs.
- Permeability estimation based on image analysis is a good alternative when an intact core-plug is not available for laboratory measurement.
- Accurately estimating permeability for carbonates, which contains highly variable pore networks, based on image analysis is still challenging.
- In this study, a method for permeability estimation based on thin-section image analysis and 2D permeability simulation was developed for grain-dominated carbonates based on semi-theoretical analysis of 2D and 3D permeability (K2D and K3D) relationships.

Sample Description

- 24 grain-dominated carbonate samples collected from six locations, and laboratory measured porosity and permeability, and thin-section based porosity and permeability

Sample	Sample location	Sample description
S11	Lower Cretaceous Thamama Group, Abu Dhabi Fields	Peloidal grain-dominated packstone, dominant tangential grain-to-grain contacts, small interparticle pores
S14		Peloidal ooid grainstone, minor amount of pore-filling cementations
S15		Peloidal ooid grainstone, minor amount of pore-filling cementations
S16		Skeletal ooid grainstone, minor amount of pore-filling cementations
S17		Skeletal ooid grainstone, minor amount of pore-filling cementations
S18		Peloidal ooid grainstone, frequent interpenetrating grain-to-grain contacts
S20		Foraminifera peloidal grain-domiated packstone, abundant equant blocky calcite cementation
S30		Skeletal peloidal grain-dominated packstone, small interparticle pores
S38		Skeletal peloidal grain-dominated packstone, small interparticle pores, including small recrystallization pores
SN12		Coated-grain ooid grainstone, minor amount of pore-filling cementations
SN15		Skeletal ooid grainstone, minor amount of pore-filling cementations
SN21		Bacinella intraclastic rudstone
SN35		Bacinella intraclastic rudstone
SN51		Skeletal peloidal grain-dominated packstone, small interparticle pores
R20	Lower Cretaceous Sligo Ooid-Shoal Complex, South-Central Texas	Skeletal coated-grain grainstone, with blocky calcite cementation
R24		Coated-grain grainstone, isopacheous bladed calcite rim-cement is abundant
R82		Ooid grainstone, with equant blocky calcite cement crystals infilling the majority of interparticle pores
L1	Ghawar Field, Saudi Arabia	Fossil grainstone with intergrain and separate-vug pore space
L2	West Texas	Medium crystalline dolostone with small intercrystal pore space
L3	West Texas	Oomoldic grainstone with cemented intergrain pores and moldic pore space
L4	Seminole Field Weste Texas	Grain-dominated dolopackstone with intergrain pore space
L5	Ghawar Field Saudi Arabia	Large crystalline dolostone with large intercrystal pores
L10	Sacroc Field West Texas	Ooid grainstone with intergrain and intragrain pore space
L15	Wasson Clear Fork field, West Texas	Medium crystalline grain-dominated dolopackstone with intergrain pore space

Sample	Measured porosity (%)	Measured permeability (mD)	Thin-section-based porosity (effective porosity) (%)	Estimated permeability (mD)
S11	23.4	7.6	5.4	12.1
S14	21.7	1615.3	11.6	1774.5
S15	21.6	2117.6	16.6	4386.6
S16	20.9	1988.7	11.6	2183.2
S17	17.8	1122.0	7.5	852.6
S18	14.3	117.2	4.8	310.3
S20	12.6	2.5	3.9	11.2
S30	22.5	11.8	7.0	4.7
S38	9.5	0.4	1.2	0.5
SN12	16.9	717.0	11.1	1880.9
SN15	17.7	2620.7	9.2	1450.0
SN21	14.6	403.8	10.9	964.4
SN35	22.5	686.5	8.3	374.5
SN51	8.6	0.1	0.7	0.1
R20	16.5	10.0	8.0	49.0
R24	17.1	8.8	10.8	40.2
R82	10.9	0.1	1.7	3.2
L1	20.0	121.0	8.7	443.5
L2	16.0	30.0	5.0	13.6
L3	25.0	5.0	1.7	23.4
L4	9.0	7.3	6.3	451.7
L5	24.0	3200.0	13.0	3335.3
L10	16.1	5.5	1.0	3.4
L15	14.2	35.0	4.5	46.5

K2D/K3D Ratio

- Kozeny-Carman (K-C) equation

One form of K-C equation is:

$$K = \frac{\emptyset r_h^2}{\beta \tau^2} \quad (1)$$

where $\emptyset$ is porosity, r_h is hydraulic radius, β is a shape factor that accounts for the influence of different shapes of the cross-sectional area, and τ is hydraulic tortuosity (L_{eh}/L_m), which is calculated as the ratio of effective hydraulic path length (L_{eh}) to minimum length along the flow path (L_m). The 2D and 3D versions of Equation 1 can be written as:

$$K_{2D} = \frac{\emptyset_{2D} {r_{h\_2D}}^2}{\beta_{2D}} \quad (2a)$$

$$K_{3D} = \frac{\emptyset_{3D} {r_{h\_3D}}^2}{\beta_{3D} \tau^2} \quad (2b)$$

Subscriptions of 2D or 3D in equations 2a and 2b denote the corresponding parameters in 2D or 3D. Hydraulic radius is defined as pore cross section area divided by cross section perimeter in 2D and pore volume divided by pore surface area in 3D, respectively:

$$r_{h\_2D} = \frac{\pi {r_{2D}}^2}{2\pi r_{2D}} \quad (3a)$$

$$r_{h\_3D} = \frac{\frac{4}{3}\pi {r_{3D}}^3}{4\pi {r_{3D}}^2} \quad (3b)$$

in which r_{2D} and r_{3D} are the equivalent pore radius from 2D and 3D image analysis, respectively. Combining equations 2 and 3 yields:

$$\frac{K_{2D}}{K_{3D}} = \frac{3}{2}\frac{\beta_{3D}}{\beta_{2D}}\frac{\emptyset_{2D}}{\emptyset_{3D}}\tau^2\frac{r_{2D}}{r_{3D}} \quad (4)$$

Assuming $<\beta_{3D}> = <\beta_{2D}>$, $<r_{2D}> = <r_{3D}>$, and $\emptyset_{2D}$ and $\emptyset_{3D}$, Equation 4 can thus be simplified to

$$\frac{K_{2D}}{K_{3D}} = \frac{3}{2}\tau^2 \quad (5)$$

With the consideration of constriction factor, Equation 5 becomes:

$$\frac{K_{2D}}{K_{3D}} = \frac{3}{2}\tau^2\frac{1}{f} \quad (6a)$$

in which

$$f = \frac{256\rho^{3.5}}{(1+\rho)^4(5\rho^3+3\rho^2+3\rho+5)} \quad (6b)$$

where $\rho = r_{min}/r_{max}$, a pore radius ratio that can be interpreted as the pore throat/pore body ratio.

Examination of the K2D/K3D Relationship

- Micro-CT scanning of sample S16

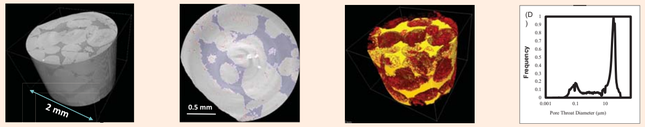

Figure 1. Caption in next column

Figure 1. Micro-CT reconstruction of sample S16 and image analysis. (A) Digital rock image of mini-plug of S16; (B) Pore segmentation. Blue shaded areas are interparticle pores, red dotted areas are intraparticle pores; (C) Interparticle and intraparticle pore network. Yellow denotes interparticle pores, and red denotes intraparticle pores. (D) Pore throat size distribution from MICP. Bimodal distribution is observed for sample S16. Right peak corresponds to interparticle pores, left peak to intraparticle pores.

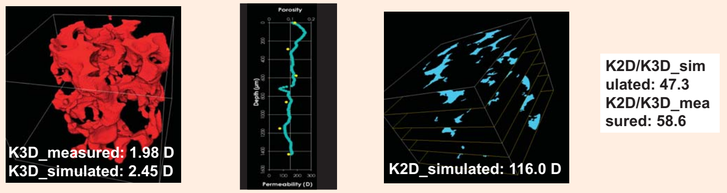

K2D/K3D_simulated: 47.3
K2D/K3D_measured: 58.6

Figure 2. Interparticle pore network 3D and 2D for sample S16. (A) 3D interparticle pore network; (B) 2D porosity and permeability along the depth within the core plug. Blue data points are porosity, orange data points are permeability; (C) Selected 2D slices along the depth having equidistance. Blue arrow denotes the direction of permeability simulation.

Comparison of K2D/K3D obtained from image analysis and based on Equation 6

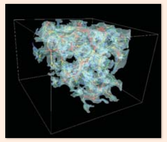

Media axis of the pore network

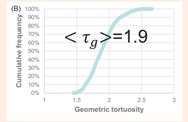

Geometric tortuosity distribution the vertical direction.

Based on Eq. 6

K2D/K3D: 24 – 61.8

Similar range with measured/simulated K2D/K3D

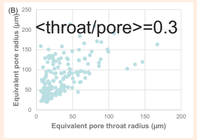

Pore throat and pore body sizes

$$\tau_h^{\ 2} = \emptyset^{1-m}$$

m = 2
τ_h = 3.0

- **Similar range of K2D/K3D is obtained, indicating the validity of using Equation 6 for K2D/K3D estimation;**
- **Uncertainty in hydraulic tortuosity estimation can be a main source of error for K2D/K3D estimation based on Equation 6.**

Permeability Estimation Based on Thin-Sections

- Thin-section pore segmentation and image analysis

Thin section **Pore segmentation**

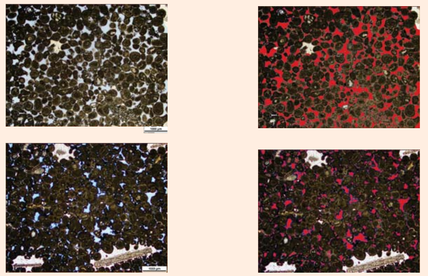

Grainstone samples with well-defined interparticle pores and minor cementation and relatively homogeneous pore distribution. K_measured: 2 D and 117.2 mD, respectively.

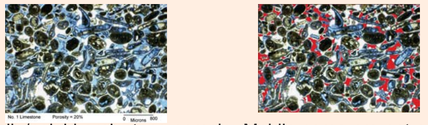

A fossile/peloid grainstone sample. Moldic pores are not counted as effective porosity that contributes significantly to permeability. K_measured: 121.0 mD.

Moldic pores and intra-particle pores need to be removed before simulation. K_measured: 1.63 mD

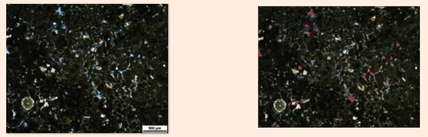

A grain-dominated packsktone with well-defined rounded peloids. K_measured: 0.1 mD.

Accurate pore segmentation is the key for permeability estimation based on thin sections

- Permeability Estimation

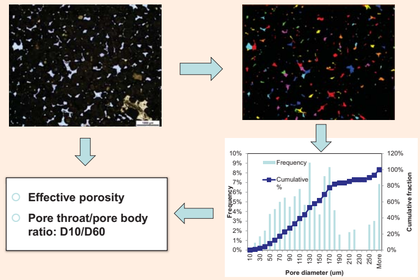

Image analysis procedure to obtain effective porosity, pore throat/pore body ratio.

Thin-section: K2D ÷ **Equation 6 and thin-section: K2D/K3D** = **K3D**

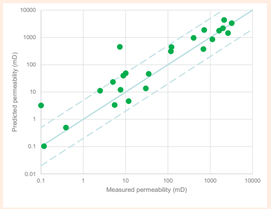

Comparison between predicted and measured permeability for the 24 samples. Solid line is the 1:1 line. The upper and lower dashed lines correspond to errors of a factor of 5 in either direction. Most permeability estimates are within a factor of ±5.

- Sources of Error

Representativeness of the thin-section

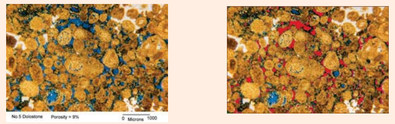

Think section and pore segmentation for sample L4. Vuggy pores are carefully identified and excluded from the effective pores. Permeability is overestimated by a factor of 62 for this sample, the largest error among the 24 samples. K_measured: 7.3 mD.
The ultra-high error is most likely caused by representativeness of the thin section, although other factors may contribute.

Correct determination of the effective pores

Thin section and pore segmentation for sample R82. K_measured: 0.1 mD.
Representativeness of this thin-section is not an issue. A more likely cause is that the pores identified as interparticle pores (red areas in right) are not dominating the flow.
Interparticle pores are isolated by the cement that make them poorly-connected and thus act as “vuggy” pores.

Other sources of error:

- Vuggy pores vs. interparticle pores – can be subjective sometimes
- Determination of D10/D60 value – affected by small pore size
- Determination of m value – a universal value of 2.0 may not be the case for different carbonate rocks; however, use of effective porosity has the effect of simplifying the pore structure that makes the m approaches to 2.0.

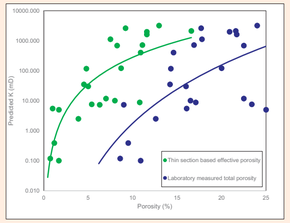

Permeability-and-porosity relationship with porosity being thin-section-based effective porosity (green data) and laboratory measured total porosity (blue data). Solid curves are power law equation fittings. R^2 is 0.67 and 0.40 for the green and orange data points, respectively. This indicates that the effective porosity is more relevant to permeability than the total porosity.

Conclusions

- The relationship between 2D and 3D permeability is evaluated mathematically based on Kozeny-Carman Equation and a constriction factor.
- This relationship was examined and validated with a grainstone sample, for which both K2D and K3D were obtained through permeability simulation based on the micro-CT images.
- The results of estimated permeability for the 24 grain-dominated carbonate samples show that 22 of them (92%) has predicted permeability within a factor of ±5 of the measured value, 44% within a factor of ±2.
- Representativeness of the thin sections and correct determination of the effective pores are the two prerequisites for reliable permeability estimation.

Acknowledgements: We thank RCRL consortium member companies for support